

CHAPTER V
**SYNTHESIS GAS PRODUCTION FROM CO₂-CONTAINING NATURAL
GAS BY COMBINED STEAM REFORMING AND PARTIAL OXIDATION
IN AN AC GLIDING ARC DISCHARGE**
(Plasma Chemistry and Plasma Processing, in press)

5.1 Abstract

In this study, a technique of combining steam reforming with partial oxidation of CO₂-containing natural gas in a gliding arc discharge plasma was investigated. The effects of several operating parameters including: hydrocarbons (HCs)/O₂ feed molar ratio; input voltage; input frequency; and electrode gap distance; on reactant conversions, product selectivities and yields, and power consumptions were examined. The results showed an increase in either methane (CH₄) conversion or synthesis gas yield with increasing input voltage and electrode gap distance, whereas the opposite trends were observed with increasing HCs/O₂ feed molar ratio and input frequency. The optimum conditions were found at a HCs/O₂ feed molar ratio of 2/1, an input voltage of 14.5 kV, an input frequency of 300 Hz, and an electrode gap distance of 6 mm, providing high CH₄ and O₂ conversions with high synthesis gas selectivity and relatively low power consumptions, as compared with the other processes (sole natural gas reforming, natural gas reforming with steam, and combined natural gas reforming with partial oxidation).

Keywords: Gliding arc discharge; Plasma; Steam reforming; Natural gas

5.2 Introduction

In the recent years, research on the natural gas conversion to synthesis gas and fuels by using reforming processes has been extensively investigated [1-6]. These studies have been based on the reforming of pure CH₄ while natural gas contains not only CH₄ but also significant amount of ethane (C₂H₆), propane (C₃H₈) and carbon dioxide (CO₂). It is known that most natural gas, with a high concentration of carbon dioxide, has been found in Asia [7]. Hence, the reforming of natural gas composed of various components without a separation process is of great interest since it can result in a reduction of the high cost of the separation process and the net emission of CO₂.

Several techniques, such as steam reforming and partial oxidation, have been developed for methane reforming; however, they still possess some problems and constraints. The most extensively investigated method for hydrogen (H₂)/synthesis gas production from methane is steam reforming. Methane reforming with steam is a direct reaction between steam and methane to achieve a gaseous product with a higher H₂ content (Equation 1). Since steam methane reforming is a highly endothermic reaction, a huge amount of supplied energy is required. The reaction normally takes place over a nickel catalyst at very high temperatures of about 425-550 °C [8].



The partial oxidation of methane is also an attractive alternative to converting methane to H₂/synthesis gas. This reaction is an exothermic reaction (Equation 2); therefore, it can reduce the energy demand for the reforming reaction [9].



Apart from the aforementioned conventional processes, non-thermal plasma is a new efficient technique, which can be used for successfully converting natural gas into synthesis gas as well as other valuable products. Under ambient temperature and pressure, it provides highly active species (electrons, ions, and free radicals), which can initiate natural gas reforming reactions [10]. The gliding arc discharge originates from an auto-oscillating phenomenon that develops between at least two

diverging electrodes submerged in a laminar or turbulent gas flow. The discharge starts as thermal plasma, and it quickly becomes non-thermal plasma during the space and time evolution. This powerful and energy-efficient transition discharge combines the benefits of equilibrium and non-equilibrium discharge characteristics in a single discharge pattern. So far, there are several research studies reporting the utilization of plasma discharge for hydrocarbon reforming [11-21]; however, to our knowledge, there have been no report on the combination of steam reforming and partial oxidation of CO₂-containing natural gas by using the gliding arc discharge system.

Therefore, the main objective of this work was to determine the roles of the gliding arc discharge plasma, in conjunction with the combined steam and partial oxidation, on the CO₂-containing natural gas reforming to produce synthesis gas. The experiments were systematically carried out to investigate the effects of several operating parameters, including the hydrocarbons (HCs)-to-O₂ feed molar ratio, input voltage, input frequency, and electrode gap distance, on reactant conversions, product selectivities and yields, and power consumptions in order to obtain optimum conditions for maximum synthesis gas production.

5.3 Experimental

5.3.1 Reactant Gases

The simulated natural gas used in this work consisted of CH₄, C₂H₆, C₃H₈, and CO₂, with a CH₄:C₂H₆:C₃H₈:CO₂ molar ratio of 70:5:5:20, and oxygen (O₂) were specially manufactured by Thai Industry Gas (Public) Co., Ltd.

5.3.2 AC Gliding Arc Discharge System

The schematic of a low-temperature gliding arc system used in this work is shown in Figure 1.

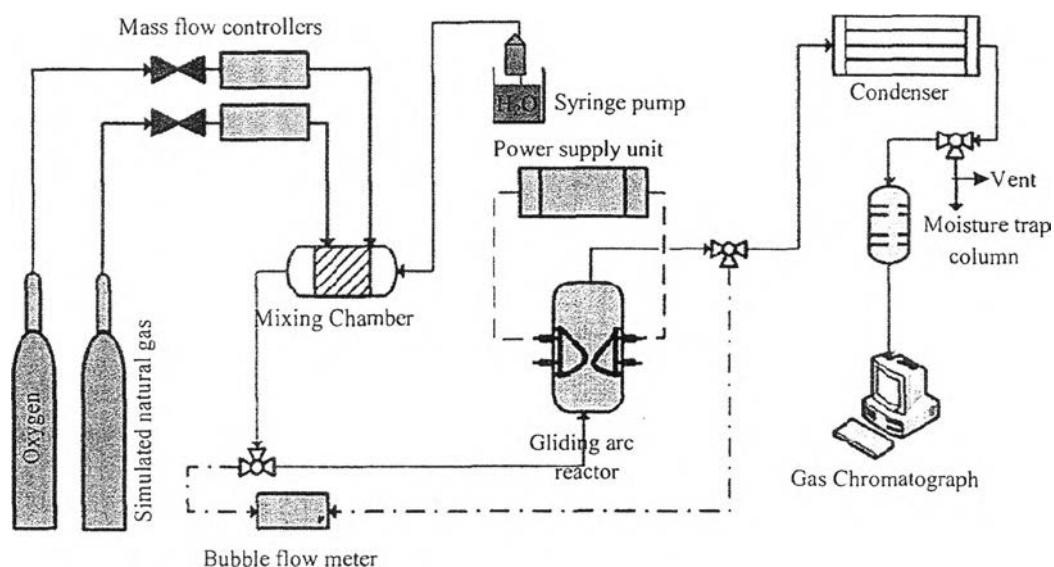


Figure 5.1 Schematic of gliding arc discharge system.

The detail of the gliding arc reactor configuration was described in our previous work [10]. The gliding arc reactor was made of a glass tube with an outer diameter of 9 cm and an inside diameter of 8.5 cm and had two diverging knife-shaped electrodes, which were made of stainless steel sheets with a 1.2 cm width. The gap distance between the pair of electrodes was fixed at 6 mm. The steam fed into the system was achieved by vaporizing water in a mixing chamber at a controlled temperature of 120 °C. The water flow rate to generate steam was controlled by a syringe pump. The flow rates of the simulated natural gas and O₂ were controlled by using mass flow controllers (98% accuracy) with transducers. A 7- μ m stainless steel filter was placed upstream of each mass flow controller in order to trap any solid particles in the reactant gases. The check valve was also placed downstream of each mass flow controller to prevent any backflow. The simulated natural gas, oxygen, and steam were well mixed in the mixing chamber before being introduced upward into the plasma reactor at atmospheric pressure. To prevent the water condensation in the feed line and plasma reactor, the temperature of stainless tube from syringe pump to the gliding arc reactor, as well as the plasma reactor itself, was maintained at 120 °C by using a heating tape. The compositions of the feed gas mixture and the outlet gas were quantitatively analyzed by an on-line gas

chromatograph (HP, 5890) equipped with two separate columns, i.e. a Carboxen 1000 packed column and a PLOT Al₂O₃ “s” capillary column, which were adequate to analyze all hydrocarbons, CO, CO₂, and H₂.

The power supply unit consisted of three steps. For the first step, a domestic AC input of 220 V and 50 Hz was converted to a DC output of 70 V by a DC power supply converter. For the second step, a 500 W power amplifier with a function generator was used to transform the DC into AC current with a sinusoidal waveform and different frequencies. For the third step, the outlet voltage was stepped up by using a high voltage transformer. The output voltage and frequency were controlled by the function generator. The voltage and current at the low voltage side were measured instead of those at the high voltage side by using a power analyzer since the plasma generated is non-equilibrium in nature. The high side voltage and current were thereby calculated by multiplying and dividing by a factor of 130, respectively [7, 8, 10, 22].

The feed gas mixture was first introduced into the gliding arc reactor without turning on the power supply unit for any studied conditions. After the compositions of outlet gas became invariant, the power supply unit was turned on. The flow rate of the outlet gas was also measured by using a bubble flow meter. The outlet gas was analyzed every 30 min by the on-line GC. After the plasma system reached a steady state with invariant outlet gas concentrations, the outlet gas was then taken for analysis at least a few times every hour. The average data were used to assess the process performance of the gliding arc discharge system.

5.3.3 Reaction Performance Calculation

The plasma system performance was evaluated from reactant conversions, product selectivities, H₂, CO, and C₂ yields, and power consumptions. The reactant conversion is defined as:

$$\% \text{ Reactant conversion} = \frac{(\text{Moles of reactant in} - \text{Moles of reactant out}) \times (100)}{\text{Moles of reactant in}} \quad (1)$$

The selectivity of any C-containing product is defined on the basis of the amount of C-containing reactants converted to any specified product, as stated in Equation 2. The percentage of coke formed can be calculated from the difference between the total reactant conversions and total C-containing products, as given in Equation 3. In the instance of the H₂ product, its selectivity is calculated based on the amount of H-containing reactants converted, as stated in Equation 4:

$$\% \text{ Selectivity for any hydrocarbon product} = \frac{[P] C_p 100}{\sum [R_i] (C_{Ri})} \quad (2)$$

$$\% \text{ Coke} = \frac{\sum [R_i] C_{Ri} - \sum [P_i] C_{Pi}}{\sum [P_i] C_{Pi}} \quad (3)$$

$$\% \text{ Selectivity for hydrogen} = \frac{[H] H_p 100}{\sum [R_i] H_{Ri}} \quad (4)$$

where [P] = moles of product in the outlet gas stream
 [R] = moles of each reactant in the feed stream to be converted
 [H] = mole of hydrogen in the outlet gas stream
 C_p = number of carbon atoms in a product molecule
 C_R = number of carbon atom in each reactant molecule
 H_p = number of H₂ atoms in a product molecule
 H_R = number of H₂ atoms in each reactant molecule

The yields of various products are calculated using the following equations:

$$\% \text{ C}_2 \text{ hydrocarbon yield} = \frac{[\sum(\% \text{ CH}_4, \% \text{ C}_2\text{H}_6, \% \text{ C}_3\text{H}_8, \% \text{ CO}_2 \text{ conversions})][\sum(\% \text{ C}_2\text{H}_2, \% \text{ C}_2\text{H}_4 \text{ selectivities})]}{(100)} \quad (5)$$

$$\% \text{ H}_2 \text{ yield} = \frac{[\sum(\% \text{ CH}_4, \% \text{ C}_2\text{H}_6, \% \text{ C}_3\text{H}_8 \text{ conversions})][\% \text{ H}_2 \text{ selectivity}]}{(100)} \quad (6)$$

$$\% \text{ CO yield} = \frac{[\sum(\% \text{ CH}_4, \% \text{ C}_2\text{H}_6, \% \text{ C}_3\text{H}_8, \% \text{ CO}_2 \text{ conversions})][\% \text{ CO selectivity}]}{(100)} \quad (7)$$

The power consumption is calculated in a unit of Ws per C-containing reactant molecule converted and Ws per H₂ molecule produced using the following equation:

$$\text{Power consumption} = \frac{P \times 60}{N \times M} \quad (8)$$

where P = power measured at the low voltage side of the power supply unit (W)

N = Avogadro's number (6.02×10^{23} molecule g mole⁻¹)

M = rate of converted carbon in the rate of produced H₂ molecules (g mole min⁻¹)

The residence time was calculated based on the reaction volume of gilding arc reactor divided by the feed flow rate. The reaction volume was estimated from the appearance of generated plasma.

5.4 Results and Discussion

In order to obtain a better understanding of the chemical reactions in a plasma environment, the possibilities of all chemical pathways, which occurred by the collisions between electrons and all reactants introduced in to the feed to produce H₂ and various hydrocarbon species are hypothesized as the following reactions [8, 10]:

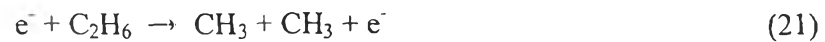
Electron-carbon dioxide collisions:



Electron-methane collisions:



Electron-ethane collisions:



Electron-propane collisions:



Electron-water collisions:



Under the presence of oxygen, several chemical reactions can be initiated in the plasma environment as follows [23]:

Dissociative attachment:



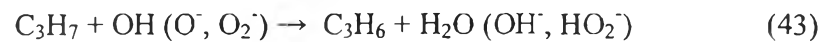
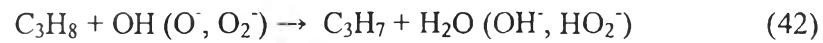
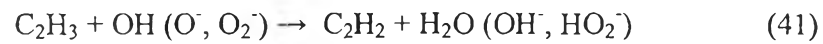
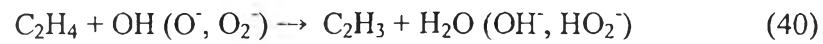
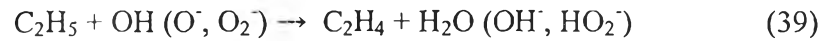
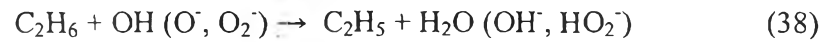
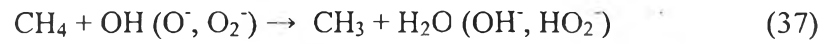
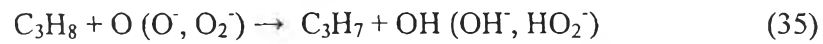
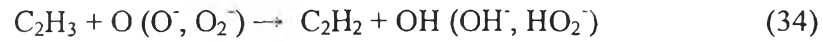
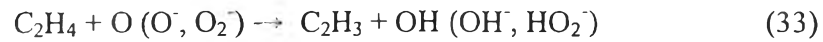
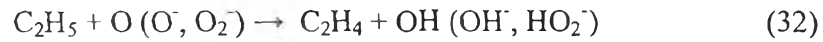
Attachment:



Dissociation:



Oxidative dehydrogenation reactions:



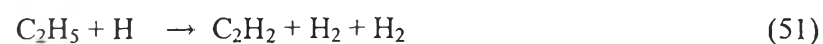
All the active species formed from either electron collisions and oxidative reactions can further react to form various products as follows:

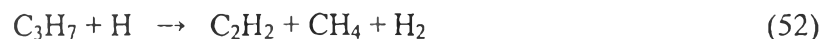
Coupling reactions of active species:

Ethylene (C₂H₄) formation;



Acetylene(C₂H₂) formation;





Butane (C₄H₁₀) formation:



Carbon monoxide (CO) formation:



5.4.1 Effect of the Hydrocarbons (HCs)-to-O₂ Feed Molar Ratio

Typically, the HCs-to-O₂ feed molar ratio in the natural gas feed mixture has a considerable impact on the plasma characteristics (i.e. breakdown voltage, electrical conductivity, and physical appearance) and the plasma stability, depending on the properties of each gas component. In this work, the experiments were initially performed by varying the O₂ content in the feed to obtain various HCs-to-O₂ feed molar ratios of 2/1, 3/1, 4/1, 6/1, and 9/1, while the other operating parameters were controlled at the base conditions (a steam content of 10 mol%, a total feed flow rate of 100 cm³/min, an input voltage of 13.5 kV, an input frequency of 300 Hz, and an electrode gap distance of 6 mm) [24]. In this plasma system, a HCs-to-O₂ feed molar ratio lower than 2/1 was not investigated since it is close to the explosion zone. The main gas products were H₂, CO, C₂H₂, C₂H₄, and C₄H₁₀. Other hydrocarbon products, alcohols, ketones, aldehydes, and etc., can be formed; however, from the product analysis, they were detected in very negligibly small amounts of lower than 0.05%.

It is very interesting to verify the formation of hydrogen resulted from various plasma reactions as mentioned before and not from the decomposition of water. An additional experiment was carried out using a feed gas having either 10 mol% steam in helium or 10 mol% steam in helium with oxygen at a He-to-O₂ molar

ratio of 2/1. The studied gliding arc reactor system was operated at a feed flow rate of $100 \text{ cm}^3/\text{min}$, an input voltage of 13.5 kV, an input frequency of 300 Hz, and an electrode gap distance of 6 mm. As expected, hydrogen was not formed in the effluents of both studied feed gases, confirming that the decomposition of water cannot occur under the studied plasma conditions.

Figure 5.2-5.6 shows the process performance of the studied gliding arc system as a function of the HCs-to- O_2 feed molar ratio. A decrease in the HCs-to- O_2 molar ratio (a lower HCs-to- O_2 feed molar ratio means a higher O_2 content) significantly enhanced both the conversions of all reactants (except CO_2) and the yields of H_2 , CO , and C_2 . The results can be explained by the fact that, when O_2 presents in the plasma system, it plays an important role in providing O_2 active species from the dissociative attachment reactions, as shown in Equations 27-29. These O_2 active species can further activate all reactants by oxidative dehydrogenation reactions (Equations 30-43), leading to an increase in the conversions of CH_4 , C_2H_6 , and C_3H_8 , as well as the H_2 , CO , and C_2 yields (Figure 5.2). An increase in O_2 content in the feed (decreasing HCs/ O_2 feed molar ratio) results in the enhancement of a complete combustion reaction, leading to a decrease in CO_2 conversion.

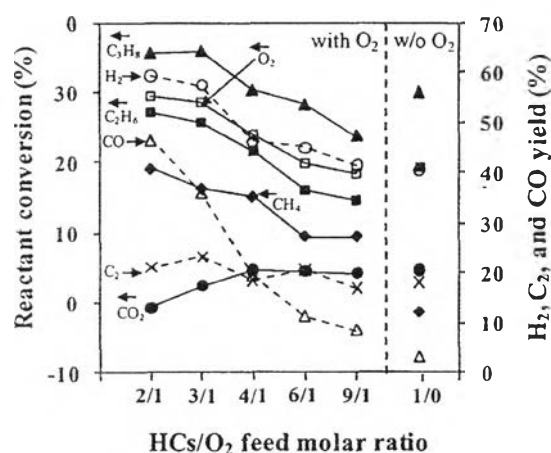


Figure 5.2 Effects of HCs-to- O_2 feed molar ratio on reactant conversions and product yields under studied conditions: steam content, 10 mol%; total feed flow rate, $100 \text{ cm}^3/\text{min}$; input voltage, 13.5 kV; input frequency, 300 Hz; and electrode

gap distance, 6 mm (E_c : power per reactant molecule converted; E_{H_2} : power per H_2 molecule produced).

As shown in Figure 5.3, the CH_4 , C_2H_6 , and C_3H_8 concentrations in the outlet gas decrease significantly with decreasing HCs-to- O_2 feed molar ratios whereas the concentration of CO increases drastically with a slight increase in H_2 concentration. Interestingly, the CO_2 conversion decreased with the decreasing HCs-to- O_2 feed molar ratio. As mentioned before, when decreasing the HCs-to- O_2 feed molar ratio, the increase in oxygen provides a higher possibility for the oxidation of hydrocarbons to CO_2 . Therefore, negative aspect of the CO_2 conversion at the lowest HCs-to- O_2 feed molar ratio of 2/1 suggests that the system provides a higher formation-rate of CO_2 by the complete hydrocarbon oxidation than the CO_2 reduction rate by the reforming reactions [10]. In comparisons between the two cases of without and with O_2 addition in the feed, the O_2 addition in the feed with any HCs-to- O_2 feed molar ratio lower than 4/1 (high O_2 content range) potentially contributes to the positive effect of the enhancement of the reactant conversions, with the exception of the CO_2 conversion, and the H_2 , CO, and C_2 yields, as well as the H_2 and CO selectivities

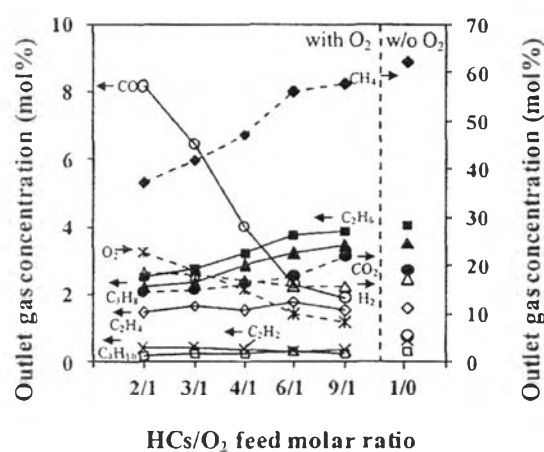


Figure 5.3 Effects of HCs-to- O_2 feed molar ratio on concentrations of outlet gas under studied conditions: steam content, 10 mol%; total feed flow rate, $100 \text{ cm}^3/\text{min}$;

input voltage, 13.5 kV; input frequency, 300 Hz; and electrode gap distance, 6 mm (E_c : power per reactant molecule converted; E_{H_2} : power per H_2 molecule produced).

The effect of the HCs-to- O_2 feed molar ratio on product selectivities is shown in Figure 5.4. The selectivities for C_2H_4 , C_4H_{10} , and H_2 tended to decrease with the decreasing HCs-to- O_2 feed molar ratio, whereas the CO selectivity increased drastically. As mentioned earlier, the higher the number of oxygen active species, the higher the opportunity for oxidative dehydrogenation reactions, consequently producing several intermediated species and water. Some of intermediate species (i.e. C_2H_5 and C_2H_3) can be further reacted to form C_2H_4 and C_2H_2 either by electron collisions (Equations 18, 20) and/or by oxidative dehydrogenation reactions (Equations 32, 34). In addition, the radicals of hydrocarbons and hydrogen derived from the earlier reactions may possibly react further to combine with one another via coupling reactions to form H_2 , C_2H_2 , C_2H_4 , and C_4H_{10} , as shown in Equations 44-54. Hence, with the decreasing tendencies of the H_2 , C_2H_2 , C_2H_4 , and C_4H_{10} selectivities with decreasing HCs-to- O_2 feed molar ratios infer that the opportunity for coupling reactions to form higher hydrocarbon molecules is less favorable at a lower HCs-to- O_2 feed molar ratio. The increase in the CO selectivity with decreasing HCs-to- O_2 feed molar ratio can be explained by the fact that the higher O and OH active species may possibly provide a higher possibility of the partial oxidative pathways forming CO as an end product (Equations 55-59).

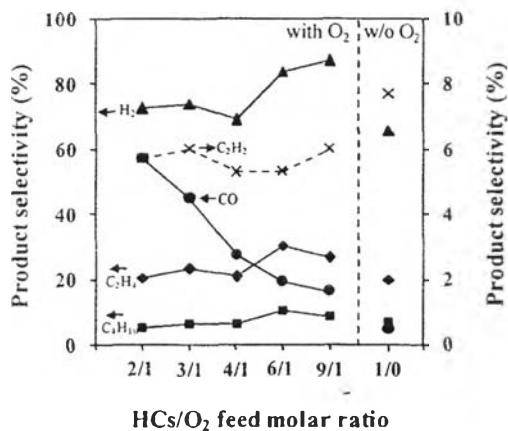


Figure 5.4 Effects of HCs-to-O₂ feed molar ratio on product selectivities under studied conditions: steam content, 10 mol%; total feed flow rate, 100 cm³/min; input voltage, 13.5 kV; input frequency, 300 Hz; and electrode gap distance, 6 mm (E_c : power per reactant molecule converted; E_{H_2} : power per H₂ molecule produced).

Figure 5.5 shows the effects of the HCs-to-O₂ feed molar ratio on various product molar ratios. The molar ratios of H₂/CO, H₂/C₂H₂, and C₂H₄/C₂H₂ tended to decrease with decreasing HCs-to-O₂ feed molar ratios, while the H₂/C₂H₄ molar ratio showed the opposite trend. These results correspond well to the decreases in the H₂, C₂H₄, and C₄H₁₀ selectivities and the increase in the CO selectivity with the decreasing HCs-to-O₂ feed molar ratio. The increase in the H₂/C₂H₄ molar ratio with the increasing O₂ ratio in the system (decreasing the HCs-to-O₂ feed molar ratio) implies that the oxidative dehydrogenation reactions of hydrocarbons to form smaller hydrocarbon molecules have higher possibilities to simultaneously occur, as compared to the coupling reactions of active species to form large hydrocarbon molecules.

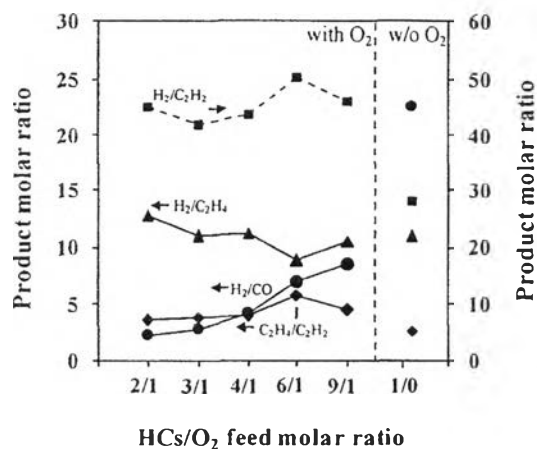


Figure 5.5 Effects of HCs-to-O₂ feed molar ratio on product molar ratios under studied conditions: steam content, 10 mol%; total feed flow rate, 100 cm³/min; input voltage, 13.5 kV; input frequency, 300 Hz; and electrode gap distance, 6 mm (E_c : power per reactant molecule converted; E_{H_2} : power per H₂ molecule produced).

The effects of the HCs-to-O₂ feed molar ratio on power consumptions and coke formation are illustrated in Figure 5.6. The power consumptions of both per reactant molecule converted and per H₂ molecule produced declined drastically with the decreasing HCs-to-O₂ feed molar ratio. The drop in both power consumptions can be explained by the increases in the CH₄, C₂H₆, and C₃H₈ conversions and H₂ yield (Figure 5.2). Moreover, a decreasing tendency of coke deposition on the electrode surfaces and inner reactor glass wall could be observed at lower HCs-to-O₂ feed molar ratios (with higher O₂ contents). From the overall results, the optimum HCs-to-O₂ feed molar ratio of 2/1, which reasonably provided both higher H₂ yield and selectivity with extremely low power consumptions, was selected for further investigation. It is interesting to point out that the addition of oxygen cannot reduce the power consumption but it can significantly decrease coke formation.

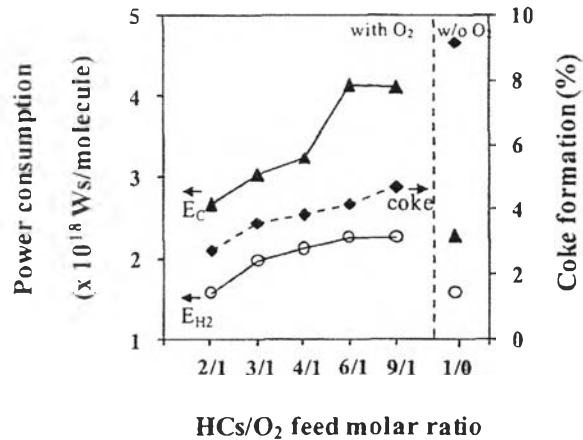


Figure 5.6 Effects of HCs-to-O₂ feed molar ratio on power consumptions and coke formation under studied conditions: steam content, 10 mol%; total feed flow rate, 100 cm³/min; input voltage, 13.5 kV; input frequency, 300 Hz; and electrode gap distance, 6 mm (E_c: power per reactant molecule converted; E_{H2}: power per H₂ molecule produced).

5.4.2 Effect of Input Voltage

In general, the input voltage plays a significant role on plasma behaviors and subsequent plasma chemical reaction performance. For the investigated plasma system, the highest operating input voltage of 20.5 kV was limited by the plasma instability and thereby the extinction of gliding arc discharges due to a very large amount of rapid coke deposited on the electrode surface. The lowest input voltage (break-down voltage) to generate steady plasma was found at 13.5 kV. Hence, the experiments were carried out to investigate the effect of input voltage in the range of 13.5-20.5 kV, while the other operating parameters were kept constant at a steam content of 10 mol%, a HCs-to-O₂ feed molar ratio of 2/1, a total feed flow rate of 100 cm³/min, an input frequency of 300 Hz, and an electrode gap distance of 6 mm. The effects of input voltage on the reactant conversions and product yields are demonstrated in Figure 5.7. The conversions of CH₄, C₂H₆, C₃H₈, and O₂, as well as the H₂ and CO yields, steadily increased with increasing input voltage. However, the CO₂ conversion remained almost unchanged in the studied

range of input voltage. These reactant conversion results were consistent with the decreases in the CH_4 , C_2H_6 , C_3H_8 , and O_2 concentrations in the outlet gas, as well as the increases in H_2 and CO concentrations (Figure 5.8). Fundamentally, an increase in the input voltage for a plasma system directly corresponds to a stronger electric field strength across the electrodes, resulting in higher electron density or higher input energy (current) to the system [10], as indicated in Figure 5.9. Increasing input voltage leads to an increased opportunity for the occurrence of elementary chemical reactions by electron collision, by resulting in increases in all the conversions of CH_4 , C_2H_6 , C_3H_8 , and O_2 , as well as the H_2 and CO yields. The unchanged CO_2 conversion and CO_2 concentration in the product gas suggest that the rate of CO_2 reforming by plasma should be equal to the rate of CO_2 formation by the complete combustion reaction. In the input voltage range of 18.5-20.5 kV, the slight increases in the CH_4 , C_2H_6 , C_3H_8 , and O_2 conversions and the H_2 and CO yields can be credited to the increase in coke formation (as shown later), which was observed to be an obstacle to maintaining steady plasma behavior. Besides, it was found that increasing input voltage had an insignificant impact on the C_2 yield, possibly, suggesting that the C_2 yield was independent of an input voltage in the investigated range.

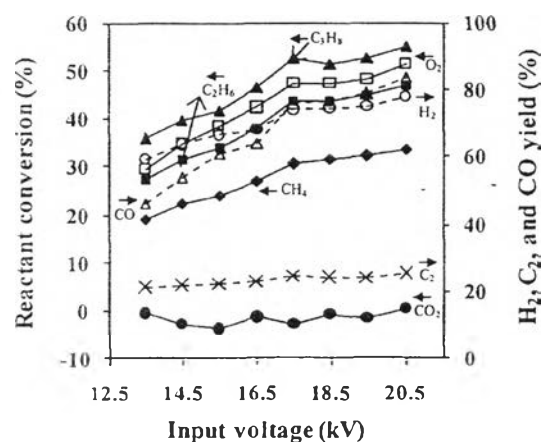


Figure 5.7 Effects of input voltage on reactant conversions and product yields under studied conditions: steam content, 10 mol%; HCs/ O_2 feed molar ratio, 2/1; total feed flow rate, $100 \text{ cm}^3/\text{min}$; input frequency, 300 Hz; and electrode gap distance, 6 mm (E_c : power per reactant molecule converted; E_{H_2} : power per H_2 molecule produced).

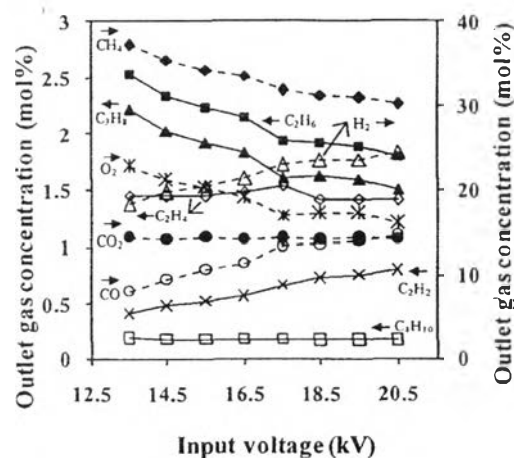


Figure 5.8 Effects of input voltage on concentrations of outlet gas under studied conditions: steam content, 10 mol%; HCs/O₂ feed molar ratio, 2/1; total feed flow rate, 100 cm³/min; input frequency, 300 Hz; and electrode gap distance, 6 mm (E_c : power per reactant molecule converted; E_{H_2} : power per H₂ molecule produced).

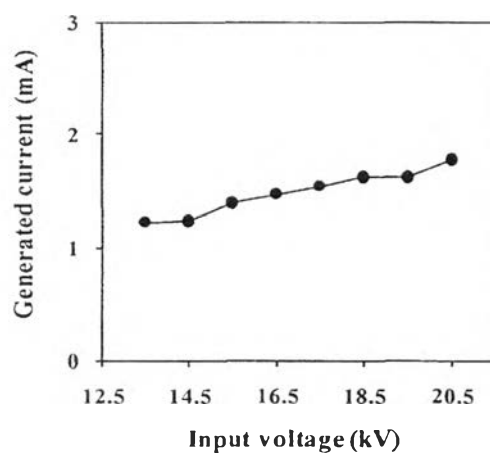


Figure 5.9 Effects of input voltage on generated current under studied conditions: steam content, 10 mol%; HCs/O₂ feed molar ratio, 2/1; total feed flow rate, 100 cm³/min; input frequency, 300 Hz; and electrode gap distance, 6 mm (E_c : power per reactant molecule converted; E_{H_2} : power per H₂ molecule produced).

Figure 5.10 presents the effects of input voltage on the product selectivities. The H₂, C₂H₄, and C₄H₁₀ selectivities decreased with increasing input voltage, whereas the C₂H₂ and CO selectivities tended to increase. These results

imply that at a higher input_voltage, the carbon dioxide dissociation by electron collision (Equations 9 and 10) and oxidative dehydrogenation reactions of the hydrocarbons (Equations 30-43) occur more often than the coupling reactions of active species (Equations 44-54). According to the plasma behavior observed, a higher input voltage can induce greater electron density and subsequently a higher number of active species, which can increased opportunity for both carbon dioxide dissociation and oxidative dehydrogenation reactions.

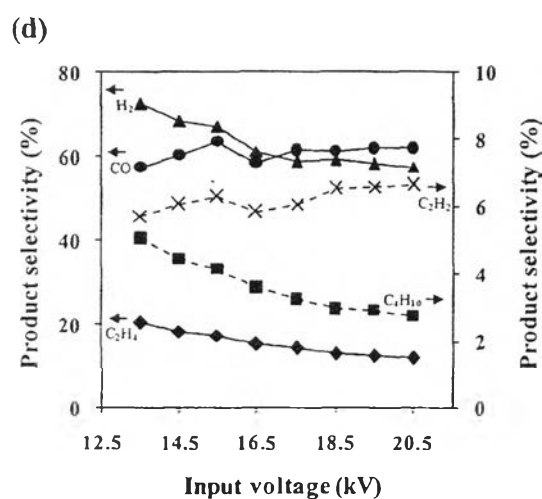


Figure 5.10 Effects of input voltage on product selectivities under studied conditions: steam content, 10 mol%; HCs/O₂ feed molar ratio, 2/1; total feed flow rate, 100 cm³/min; input frequency, 300 Hz; and electrode gap distance, 6 mm (E_c : power per reactant molecule converted; E_{H_2} : power per H₂ molecule produced).

The effect of input voltage on the product molar ratios is illustrated in Figure 5.11. The molar ratios of H₂/CO, H₂/C₂H₂, and C₂H₄/C₂H₂ substantially decreased with increasing input voltage, while the H₂/C₂H₄ molar ratio showed the opposite trend. These results agree well with the decreased H₂, C₂H₄, and C₄H₁₀ selectivities and the increased C₂H₂ and CO selectivities. The apparent decreases in the H₂/C₂H₂, H₂/CO, and C₂H₄/C₂H₂ molar ratios, and the opposite trend of the H₂/C₂H₄ molar ratio with increasing input voltage, again confirm that the carbon dioxide dissociation by electron collision and oxidative dehydrogenation reactions are much

more likely to occur than the coupling reactions of active species with increasing input voltage.

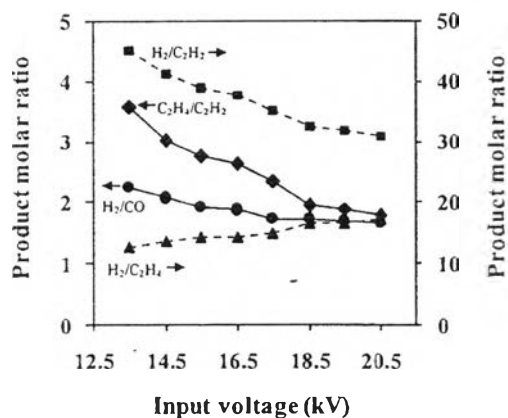


Figure 5.11 Effects of input voltage on product molar ratios under studied conditions: steam content, 10 mol%; HCs/O₂ feed molar ratio, 2/1; total feed flow rate, 100 cm³/min; input frequency, 300 Hz; and electrode gap distance, 6 mm (E_c : power per reactant molecule converted; E_{H_2} : power per H₂ molecule produced).

Figure 5.12 shows the effects of input voltage on power consumptions and coke formation. The power consumptions of both per reactant molecule converted and per H₂ molecule produced, decreased with increasing input voltage (from 13.5 to 14.5 kV); however, with further increasing input voltage to 20.5 kV, the power consumption per reactant molecule converted tended to be fairly constant, while the power consumption per H₂ molecule produced tended to only slightly increase. The initial decreases in both amounts of power consumptions can be explained by the increases in the CH₄, C₂H₆, and C₃H₈ conversions and the H₂ yield with increasing input voltage. When considering the input voltage range of 14.5-20.5 kV, the results reveal that the power consumption per H₂ molecule produced increased steadily with increasing input voltage. The increase in H₂ yield with increasing input voltage should indeed have led to lower power consumption per H₂ molecule produced. However, the opposite trend was experimentally observed, possibly because of the increase in coke formation. Generally, the formation of coke along the knife-shaped electrodes at high input voltages not only decreases the

efficiency of chemical reactions (i.e. decreasing rate of increasing reactant conversions and product yields) but also directly affects the gliding arc discharge stability. Particularly, an increase in a certain amount of coke can increase the conductivity of the system, leading to a decrease in the uniformity of the plasma pattern. This phenomena resulted in a lowered probability of electron collision with reactant molecules to produce active gaseous species. From the results, a minimum of power consumptions were found at the input voltage of 14.5 kV, while all ratios of hydrogen-to-other products were mostly high; therefore, the input voltage of 14.5 kV was selected for further investigation.

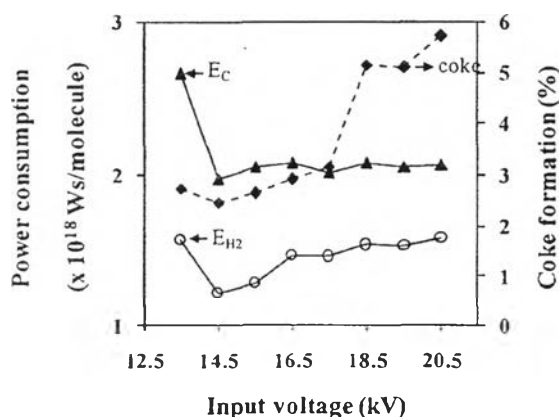


Figure 5.12 Effects of input voltage on power consumptions and coke formation under studied conditions: steam content, 10 mol%; HCs/O₂ feed molar ratio, 2/1; total feed flow rate, 100 cm³/min; input frequency, 300 Hz; and electrode gap distance, 6 mm (E_c : power per reactant molecule converted; E_{H_2} : power per H₂ molecule produced).

5.4.3 Effect of Input Frequency

The input frequency parameter was next investigated by varying the range from 290-500 Hz, while the other operating parameters were controlled at a steam content of 10 mol%, a HCs/O₂ feed molar ratio of 2/1, a total feed flow rate of 100 cm³/min, an input voltage of 14.5 kV, and an electrode gap distance of 6 mm. It should be noted that the studied gliding arc system could not be operated lower than the lowest operating input frequency of 290 Hz. This is because a large amount of

coke formation occurred on the surface of the electrodes as well as the extremely high current. For the input frequency greater than 500 Hz, the plasma system could not be operated because of the non-uniform plasma with a extremely small number of arcs produced. Figure 5.13-5.18 illustrates the effects of input frequency on the reactant conversions, product yields, concentrations of outlet gas, and power consumptions. The conversions of CH_4 , C_2H_6 , C_3H_8 , and O_2 , as well as the H_2 , CO , and C_2 yields, tended to decrease with increasing input frequency (Figure 5.13). These results correspond well to the increases in CH_4 , C_2H_6 , C_3H_8 , and O_2 concentrations, as well as the decreases in H_2 and CO concentrations in the outlet gas (Figure 5.14). In general, for any given input voltage and electrode gap distance, the electric current required to sustain a discharge is reduced with increasing input frequency. Consequently, a lower current can be observed at a higher input frequency, as shown in Figure 5.15. In accordance with the basic concept of the frequency effect as stated, the space charge (electrons and ions) characteristics of the alternating current discharge is the influential factor of frequency in changing the behaviors of arc discharge and reaction performance [8, 10, 25-26]. Therefore, increasing input frequency adversely causes a reduction in the number of electrons generated for initiating the chemically active species via the elementary plasma reactions by electron impact, resulting in lower reactant conversions and product yields.

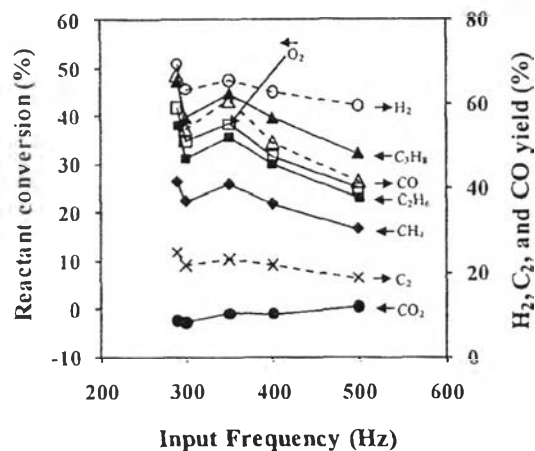


Figure 5.13 Effects of input frequency on reactant conversions and product yields, under studied conditions: steam content, 10 mol%; HCs/O₂ feed molar ratio, 2/1; total feed flow rate, 100 cm³/min; input voltage, 14.5kV; and electrode gap distance, 6 mm (E_c : power per reactant molecule converted; E_{H_2} : power per H₂ molecule produced).

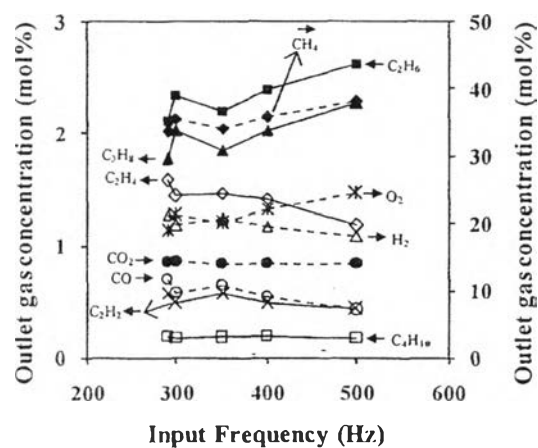


Figure 5.14 Effects of input frequency on concentrations of outlet gas under studied conditions: steam content, 10 mol%; HCs/O₂ feed molar ratio, 2/1; total feed flow rate, 100 cm³/min; input voltage, 14.5kV; and electrode gap distance, 6 mm (E_c : power per reactant molecule converted; E_{H_2} : power per H₂ molecule produced).

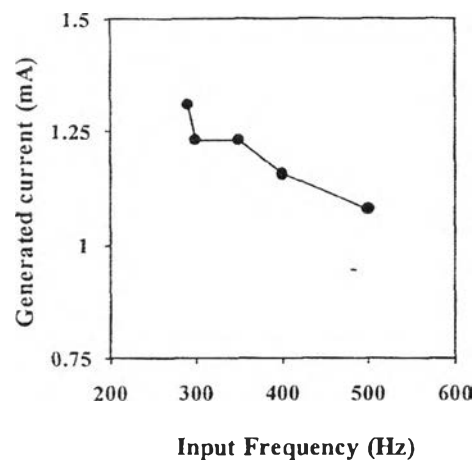


Figure 5.15 Effects of input frequency on generated current under studied conditions: steam content, 10 mol%; HCs/O₂ feed molar ratio, 2/1; total feed flow rate, 100 cm³/min; input voltage, 14.5kV; and electrode gap distance, 6 mm (E_c : power per reactant molecule converted; E_{H_2} : power per H₂ molecule produced).

The effect of input frequency on the product selectivities is shown in Figure 5.16. The H₂, C₂H₂, and C₄H₁₀ selectivities tended to increase with increasing input frequency from 290 to 500 Hz, whereas the C₂H₄ and CO selectivities tended to remain almost unchanged, implying that the C₂H₄ and CO selectivities were independent of input frequency. The present results do not agree with those in our previous work [10], in which the decreases in both H₂ and C₂H₂ selectivities were observed with increasing input frequency from 250-500 Hz. The difference in the experimental results could possibly be explained by the fact that the previous work used only simulated natural gas as a reactant feed, whereas the present work was conducted by adding both steam and oxygen to the simulated natural gas. Hence, the results imply that the presence of steam and oxygen plays an important role in enhancing the electron-water collisions (Equations 25 and 26), as well as the dissociation reactions of oxygen (Equations 27-29), leading to increased oxidative dehydrogenation reactions (Equations 30-43) and coupling reactions of active species (Equations 44-54) to produce more H₂ and C₂H₂. As shown in Figure 5.16, the

increase in C_4H_{10} selectivity infers that the promotion of coupling reactions to form C_4H_{10} (Equations 53 and 54) can be achieved by increasing input frequency.

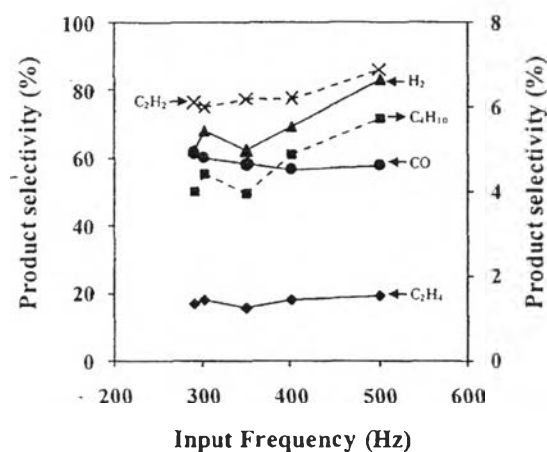


Figure 5.16 Effects of input frequency on product selectivities under studied conditions: steam content, 10 mol%; HCs/ O_2 feed molar ratio, 2/1; total feed flow rate, 100 cm^3/min ; input voltage, 14.5kV; and electrode gap distance, 6 mm (E_c : power per reactant molecule converted; E_{H_2} : power per H_2 molecule produced).

Figure 5.17 shows the effect of input frequency on the product molar ratios. The molar ratios of H_2/CO and H_2/C_2H_2 tended to increase with increasing input frequency. The increase in the H_2/CO molar ratio can be possibly described by the increase in the H_2 selectivity, while the CO selectivity remained almost unchanged with increasing input frequency. Interestingly, the simultaneous increases in the H_2/C_2H_2 molar ratio and the H_2 and C_2H_2 selectivities imply that the increase in the H_2 production rate is higher than that of the C_2H_2 production rate where the input frequency is increased. As a result, the number of electrons generated in the plasma system decreases with increasing input frequency, resulting in decreasing possibilities of secondary dehydrogenation reactions of hydrocarbon species (Equations 30-34 and 37-41) to produce C_2H_2 . On the contrary, the H_2 selectivity increase with increasing input frequency is possibly due to the presence of steam, which provides a higher possibility of collision, between the electrons and water molecules (Equations 25-26). In addition, the C_2H_4/C_2H_2 molar ratio decreased

slightly with increasing input frequency, whereas the $\text{H}_2/\text{C}_2\text{H}_2$ molar ratio remained almost unchanged. These results agree well with the increase in C_2H_2 selectivity and the invariant of C_2H_4 selectivity.

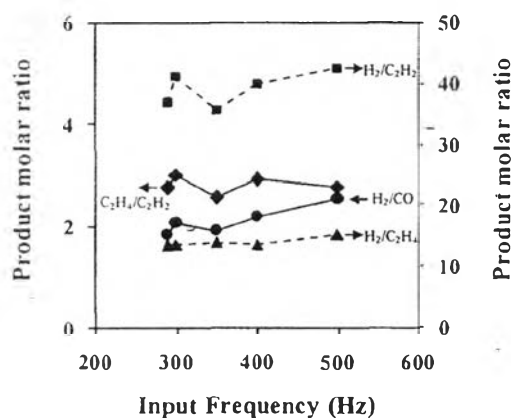


Figure 5.17 Effects of input frequency on product molar ratios under studied conditions: steam content, 10 mol%; HCs/O_2 feed molar ratio, 2/1; total feed flow rate, $100 \text{ cm}^3/\text{min}$; input voltage, 14.5kV; and electrode gap distance, 6 mm (E_c : power per reactant molecule converted; E_{H_2} : power per H_2 molecule produced).

The effects of input frequency on power consumptions and coke formation are depicted in Figure 5.18. The power consumptions of both per reactant molecule converted and per H_2 molecule produced initially decreased with increasing input frequency from 290 to 300 Hz and then substantially increased with further increasing input frequency from 300 to 500 Hz. The initial decrease in both power consumptions was observed probably due to the decrease in current required to sustain the discharge (Figure 5.15); whereas the further increase in input frequency from 300 to 500 Hz increased both power consumptions, probably resulting from the decreases in all reactant conversions and H_2 yield and selectivity (Figure 5.13). Interestingly, power consumptions mirrored the coke formation profile, suggesting that coke deposition plays a significant role in affecting the power consumptions. From the results, lower power consumptions occurred with less coke formation were found at the input frequency of 300 Hz. It was selected as an optimum value for further investigation.

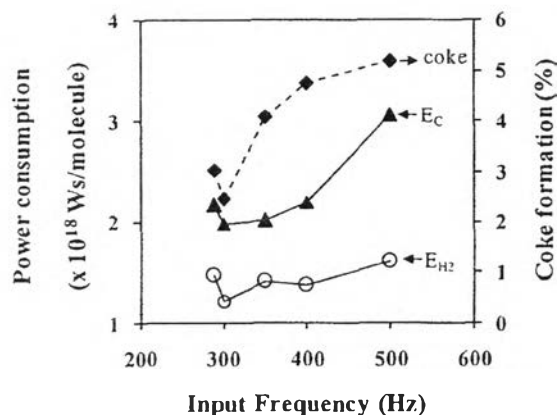


Figure 5.18 Effects of input frequency on power consumptions and coke formation under studied conditions: steam content, 10 mol%; HCs/O₂ feed molar ratio, 2/1; total feed flow rate, 100 cm³/min; input voltage, 14.5kV; and electrode gap distance, 6 mm (E_c : power per reactant molecule converted; E_{H_2} : power per H₂ molecule produced).

5.4.4 Effect of Electrode Gap Distance

For the investigation of the effect of electrode gap distance on the reforming reaction performance of the simulated natural gas, the electrode gap distance was varied in the range of 4-8 mm, while a steam content of 10 mol%, a HCs-to-O₂ feed molar ratio of 2/1, a total feed flow rate of 100 cm³/min, an input voltage of 14.5 kV, and input frequency of 300 Hz were used as the optimum conditions to operate the gliding arc system. The corresponding residence times at various electrode gap distances of 4, 6, 7, and 8 mm were 1.09, 1.37, 1.57, and 1.65 s, respectively. Beyond the highest electrode gap distance of 8 mm, the gliding arc system could not provide a steady discharge, whereas, at any electrode gap distance shorter than 4 mm, the system produced a large quantity of coke filaments across the two electrodes with in a relatively short operation period, causing a drastic drop of current and the termination of discharge.

The effects of the electrode gap distance on the reactant conversions and product yields are illustrated in Figure 5.19. The conversions of CH₄, C₂H₆, C₃H₈, and O₂, as well as the H₂, CO, and C₂ yields, significantly increased with

increasing electrode gap distance from 4 to 7 mm. The increase in the electrode gap distance simply increases the reaction volume and subsequently the residence time of gaseous species in the plasma zone increases. As a result, there is higher possibility of collisions between reactant molecules and electrons, leading to increases in all the reactant conversions (except CO_2) and product yields. These results are in good agreement with the significant decreases in the CH_4 , C_2H_6 , C_3H_8 , and O_2 concentrations and the increases in the H_2 and CO concentrations in the outlet gas (Figure 5.20). However, it was found that increasing the electrode gap distance in the range of 7-8 mm only slightly increased the CH_4 , C_2H_6 , C_3H_8 , and O_2 conversions, as well as H_2 , CO , and C_2 yields. It should be noted that there is another vital factor, apart from residence time, that affects the reactant conversions, product selectivities, and yields. When the electrode gap distance is varied, principally, the breakdown voltage required for initiating the plasma discharges and the power required for sustaining the discharges increase with increasing electrode gap distance [27]. However, if the electrode gap distance is too wide, the electric field strength weakens, resulting in a lower average electron energy, as well as a reduction in the number of electrons, which corresponds very well with the decreasing tendency of the generated current in the electrode gap distance range of 6 to 8 mm, as clearly shown in Figure 5.21. Hence, all reactant conversions and product yields remained almost unchanged with increasing gap distance in this range, despite a longer residence time. Moreover, the results of the reactant conversions and product yields at different ranges of electrode gap widths indicate that for the narrow electrode gap distance range of 4-6 mm, the residence time plays a dominant role in enhancing the plasma reforming performance, whereas, for the greater electrode gap distance range of 6-8 mm, the discharge characteristics have more significant impacts.

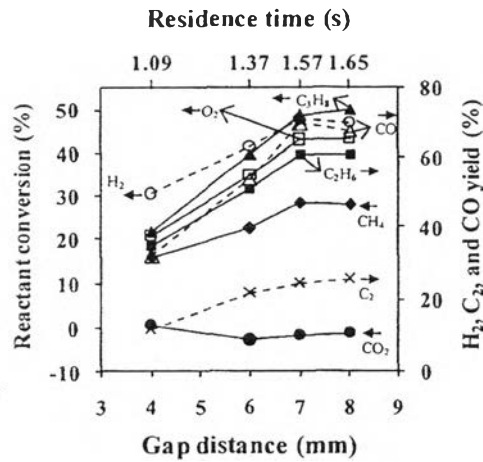


Figure 5.19 Effects of electrode gap distance on reactant conversions and product yields under studied conditions: steam content, 10 mol%; HCs/O₂ feed molar ratio, 2/1; total feed flow rate, 100 cm³/min; input voltage, 14.5 kV; and input frequency, 300 Hz (E_c : power per reactant molecule converted; E_{H_2} : power per H₂ molecule produced).

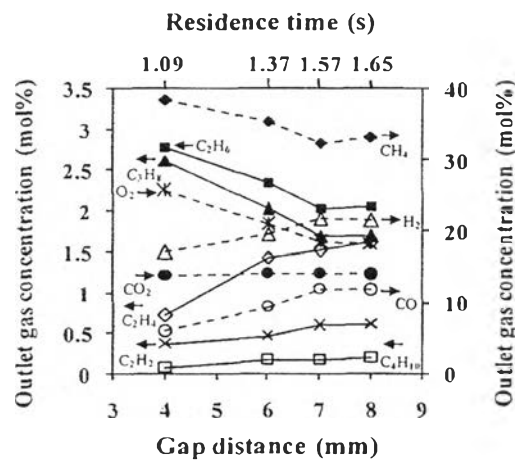


Figure 5.20 Effects of electrode gap distance on concentrations of outlet gas, (c) generated current under studied conditions: steam content, 10 mol%; HCs/O₂ feed molar ratio, 2/1; total feed flow rate, 100 cm³/min; input voltage, 14.5 kV; and input frequency, 300 Hz (E_c : power per reactant molecule converted; E_{H_2} : power per H₂ molecule produced).

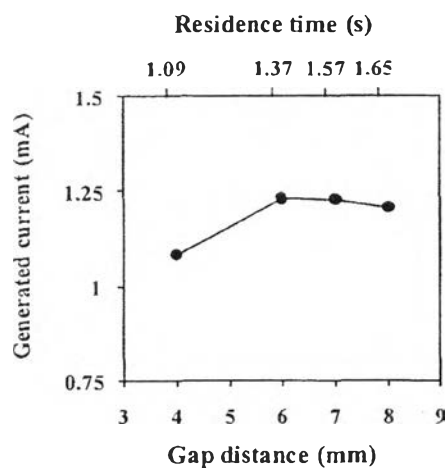


Figure 5.21 Effects of electrode gap distance on generated current under studied conditions: steam content, 10 mol%; HCs/O₂ feed molar ratio, 2/1; total feed flow rate, 100 cm³/min; input voltage, 14.5 kV; and input frequency, 300 Hz (E_c : power per reactant molecule converted; E_{H_2} : power per H₂ molecule produced).

Figure 5.22 presents the effect of electrode gap distance on the product selectivities. The H₂ and C₂H₂ selectivities significantly decreased with increasing electrode gap distance. It may be implied that the increase in current by tapering electrode gap distance is responsible for the enhancement of the oxidative dehydrogenation reactions and the coupling reactions of the active species to form H₂ and C₂H₂. On the other hand, the C₂H₄ and C₄H₁₀ selectivities tended to slightly increase with the expansion of electrode gap distance from 4 to 6 mm but beyond the electrode gap distance of 6 mm, they slightly decreased. These initial increases in both the C₂H₄ and C₄H₁₀ selectivities suggest that the coupling reactions to obtain C₂H₄ and C₄H₁₀ (Equations 44-47 and 53-54) more favorably occur than with the oxidative dehydrogenation reactions at a wider electrode gap distance (a longer residence time). A plausible explanation is that with wider electrode gap distance, the active species of hydrocarbons can further recombine via the coupling reactions due to the increase in residence time. However, when widening the electrode gap distance from 6 to 8 mm, all the product selectivities tended to slightly decrease probably due to both the decrease in generated current, as described earlier, and the drastic increase in coke formation, as shown next. The CO selectivity varied slightly

with a wider electrode gap distance, suggesting that the CO selectivity is independent of the electrode gap distance under the studied conditions.

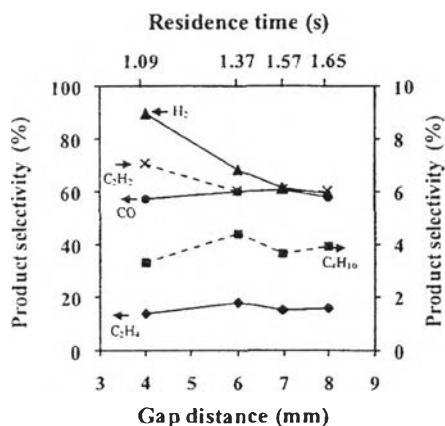


Figure 5.22 Effects of electrode gap distance on product selectivities under studied conditions: steam content, 10 mol%; HCs/O₂ feed molar ratio, 2/1; total feed flow rate, 100 cm³/min; input voltage, 14.5 kV; and input frequency, 300 Hz (E_c : power per reactant molecule converted; E_{H_2} : power per H₂ molecule produced).

Figure 5.23 illustrates the effect of the electrode gap distance on various product molar ratios. The molar ratios of H₂/CO, H₂/C₂H₂, and H₂/C₂H₄ greatly decreased with increasing electrode gap distance from 4 to 6 mm and then only slightly decreased with further widening of the electrode gap distance to 8 mm, whereas the C₂H₄/C₂H₂ molar ratio showed the opposite trend. These results again confirm that the coupling reactions of the active species more preferentially occur as secondary reactions than the dehydrogenation reactions when the system is operated at a longer residence time.

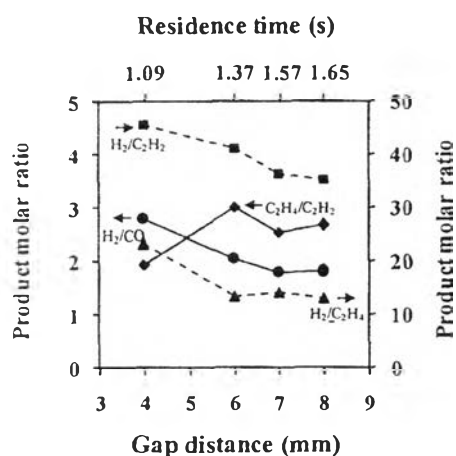


Figure 5.23 Effects of electrode gap distance on product molar ratios under studied conditions: steam content, 10 mol%; HCs/O₂ feed molar ratio, 2/1; total feed flow rate, 100 cm³/min; input voltage, 14.5 kV; and input frequency, 300 Hz (E_c : power per reactant molecule converted; E_{H_2} : power per H₂ molecule produced).

The power consumptions both per reactant molecule converted and per H₂ molecule produced decrease significantly with widening electrode gap distance from 4 to 6 mm and they tend to increase slightly with further widening of the electrode gap distance from 6 to 8 mm, as depicted in Figure 5.24. The initial decrease in both power consumptions can be explained by the increases in the CH₄, C₂H₆, C₃H₈, and O₂ conversions, as well as the H₂ yield (Figure 5a). Beyond the electrode gap distance of 6 mm, which provided the minimum power consumptions, an increase in coke formation with further widening electrode gap distance is responsible for the increase in power consumptions.

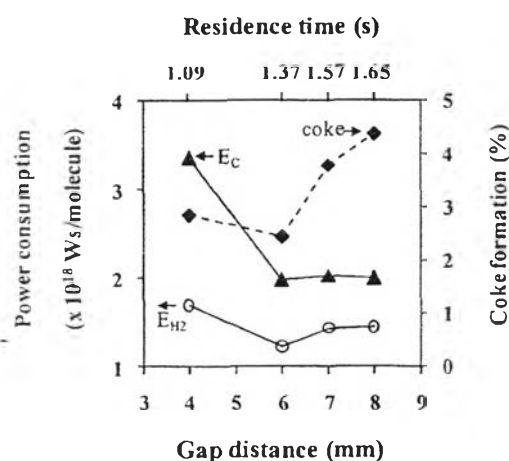


Figure 5.24 Effects of electrode gap distance on power consumptions and coke formation under studied conditions: steam content, 10 mol%; HCs/O₂ feed molar ratio, 2/1; total feed flow rate, 100 cm³/min; input voltage, 14.5 kV; and input frequency, 300 Hz (E_c : power per reactant molecule converted; E_{H_2} : power per H₂ molecule produced).

5.4.5 Comparisons of CO₂-Containing Natural Gas Conversion Performances with Different Reforming Processes

Table 5.1 shows the comparisons of CO₂-containing natural gas conversion performances, i.e. H₂ and CO selectivities and yields as well as power consumptions, with different reforming processes under their corresponding optimum conditions. It can be seen that the steam reforming process provided the highest H₂ selectivity of about 65.8%, but gave a very low CO selectivity of about 4.8%, as compared to the other reforming processes. Even though the highest H₂ selectivity was not obtained, the combined steam reforming and partial oxidation process gave acceptably high H₂ and CO selectivities of about 68.2% and 59.9%, respectively. As shown in Table 5.1, the significant enhancement of both the H₂ and CO selectivities for the combined steam reforming and partial oxidation process, as compared to all the other reforming processes. Both the steam and O₂ additions to the natural gas feed provides much higher number of oxygen active species, hydroxyl active species, and hydrogen active species (Equations 25-29). This enhances both the oxidative dehydrogenation reactions and coupling reactions (Equations 9-24, and

30-54). Interestingly, the combined steam reforming and partial oxidation process gives a very high CO production, as compared to the steam reforming process. This is because the added oxygen in the system can significantly suppress the coke formation, resulting in increased opportunities for CO formation (Equations 55-59). Hence, it can be clearly seen that the addition of both steam and oxygen can offer the acceptably highest synthesis gas production.

The power consumptions both per reactant molecule converted and per H₂ molecule produced are also given in Table 5.1. The results indicate that the presence of either oxygen (the combined reforming and partial oxidation process) or steam (the steam reforming process) in the natural gas feed could lower the power consumptions both per reactant molecule converted and per H₂ molecule produced, as compared to the case without the O₂ and steam addition (the sole reforming or non-oxidative reforming). The lowest power consumptions both per reactant molecule converted and per H₂ molecule produced were obtained from the combined steam reforming and partial oxidation process in the present work, suggesting that there is a synergistic effect of reduction in power consumption.

Table 5.1 Comparison of the CO₂-containing natural gas conversion performances with different processes under their corresponding optimum conditions

Process	Operating conditions						Selectivity (%)		Yield (%)		Power consumptions (per molecule)			
	HCs/O ₂ molar ratio	Steam content (mol%)	Total feed flow rate (cm ³ /min)	Input voltage (kV)	Input frequency (Hz)	Electrode gap distance (mm)	H ₂	CO	H ₂	CO	Per reactant molecule converted (E _C)		Per H ₂ molecule produced (E _{H₂})	
											Ws × 10 ¹⁸	eV	Ws × 10 ¹⁸	eV
Non-oxidative reforming ^a	-	-	125	15.5	300	6	24.5	2.9	12.2	-	6.34	39.58	3.58	22.35
Combined reforming and partial oxidation ^b	2/1	-	125	17.5	300	6	40.5	21.9	58.1	61.6	2.73	17.02	2.49	16.60
Steam reforming ^c	-	10	100	13.5	300	6	65.8	4.8	40.3	3.1	2.26	24.11	1.58	9.86
Combined steam reforming and partial oxidation ^d	2/1	10	100	14.5	300	6	68.2	59.9	63.4	54.0	1.98	12.36	1.22	7.62

^a[7], ^b[10], ^c[24], and ^dPresent work

5.5 Conclusions

In this work, the combined steam reforming and partial oxidation of CO₂-containing natural gas was employed for the synthesis gas production from CO₂-containing natural gas in an AC gliding arc discharge system. The effects of the input voltage, input frequency, and electrode gap distance significantly affected the reactant conversions, product selectivities, and product yields were investigated. The optimum conditions were found at a HC_s/O₂ feed molar ratio of 2/1, an input voltage of 14.5 kV, an input frequency of 300 Hz, and an electrode gap distance of 6 mm, which provided high CH₄ and O₂ conversions with high synthesis gas selectivity and very low power consumptions. Under these optimum conditions, the power consumptions were as low as 1.98×10^{-18} Ws (12.35 eV) per molecule of converted reactant and 1.22×10^{-18} Ws (7.64 eV) per molecule of produced hydrogen.

5.6 Acknowledgements

The authors would like to thank the Sustainable Petroleum and Petrochemicals Research Unit, Center for Petroleum, Petrochemicals, and Advanced Materials, Chulalongkorn University, Thailand for providing a Ph.D. scholarship for the first author and the Ratchadapisek Somphot Endowment Fund, Chulalongkorn University, Thailand for providing a financial support for this research.

5.7 References

- [1] SW. Yang, JN. Kondo, K. Hayashi, M. Hirono, K. Domen, H. Hosono. Partial oxidation of methane to syngas over promoted C12A7. *Applied Catalysis A: General* 227 (2004) 239-246.
- [2] N.R. Bruke, DL. Trimm. Co-generation of energy and synthesis gas by partial oxidation of methane. *Catalysis Today* 117 (2006) 248-252.
- [3] R.C. Vasant, C.M. Kartick. CO₂ reforming of methane combined with steam reforming or partial oxidation of methane to syngas over NdCoO₃ perovskite-type mixed metal-oxide catalyst. *Applied Energy* 83 (2006) 1024-1032.

- [4] W. Yu, T. Ohmori, S. Kataoka, T. Yamamoto, A. Endo, M. Nakaiwa, N. Itoh. A comparative simulation study of methane steam reforming in a porous ceramic membrane reactor using nitrogen and steam as sweep gases. *International Journal of Hydrogen Energy* 33 (2008) 685-692.
- [5] S. Ryi, J. Park, D. Kim, T. Kim, S. Kim. Methane steam reforming with a novel catalytic nickel membrane for effective hydrogen production. *Journal of Membrane Science* 339 (2009) 189-194.
- [6] C.R.M. Santos, M. Laureanny, B.P. Fabio. The effect of the addition of Y_2O_3 to Ni/ α - Al_2O_3 catalysts on the autothermal. *Catalysis Today* 149 (2010) 401-406.
- [7] N. Rueangjitt, C. Akarawitoo, T. Sreethawong, S. Chavadej. Reforming of CO_2 -containing natural gas using an AC gliding arc system: Effect of gas component in natural gas. *Plasma Chemistry and Plasma Processing* 27 (2007) 559-576.
- [8] T. Sreethawong, P. Thakonpatthanakun, S. Chavadej. Partial oxidation of methane with air for synthesis gas production in a multistage gliding arc discharge system. *International Journal of Hydrogen Energy* 32 (2007) 1067-1079.
- [9] J.A. Anderson, M.F. Garcia. *Supported Metals in Catalysis*. Imperial College Press, 2005.
- [10] N. Rueangjitt, T. Sreethawong, S. Chavadej. Reforming of CO_2 -containing natural gas using an AC gliding arc system: effects of operational parameters and oxygen addition in feed. *Plasma Chemistry and Plasma Processing* 28 (2008) 49-67.
- [11] B. Wang, X. Zhang, Y. Liu, G. Xu. Conversion of CH_4 , steam and O_2 to syngas and hydrocarbons via dielectric barrier discharge. *Journal of Natural Gas Chemistry* 18 (2009) 94-97.
- [12] M.G. Sobacchi, A.V. Saveliev, A.A. Fridman, L.A. Kennedy, S. Ahmed, T. Krause. Experimental assessment of combined plasma/catalytic system for hydrogen production via partial oxidation of hydrocarbon fuels. *International Journal of Hydrogen Energy* 27 (2002) 635-642.

- [13] J.X. He, Y.Y. Han, A.H. Gao, Y.S. Zhou, Z.G. Lu. Investigation on methane decomposition and the formation of C₂ hydrocarbons in DC discharge plasma by emission spectroscopy. *Chinese Journal of Chemical Engineering* 12 (2004) 149-151.
- [14] T. Nozaki, A. Hattori, K. Okazaki. Partial oxidation of methane using a microscale non-equilibrium plasma reactor. *Catalysis Today* 98 (2004) 607-616.
- [15] C.S. Kalra, A.F. Gutsol, A.A. Fridman. Gliding arc discharge as a source of intermediate plasma for methane partial oxidation. *IEEE Transactions on Plasma Science* 33 (2005) 32-4.
- [16] T. Paulmier, L. Fulcheri. Use of non-thermal plasma for hydrocarbons reforming. *Chemical Engineering Journal* 106 (2005) 59-71.
- [17] Y. Wang, C.J. Liu, Y.P. Zhang. Plasma methane conversion in the presence of dimethyl ether using dielectric-barrier discharge. *Energy & Fuels* 19 (2005) 877-881.
- [18] E. El Ahmar, C. Met, O. Aubry, A. Khacef, J.M. Cormier. Hydrogen enrichment of a methane-air mixture by atmospheric pressure plasma for vehicle applications. *Chemical Engineering Journal* 116 (2006) 13-18.
- [19] G. Petitpas, J.-D. Rollier, A. Darmon, J. Gonzalez-Aguilar, R. Matkemeijer, L. Fulcheri. A comparative study of non-thermal plasma assisted reforming technologies. *International Journal of Hydrogen Energy* 32 (2007) 2848-2867.
- [20] Y.C. Yang, B.J. Lee, Y.N. Chun. Characteristics of methane reforming using gliding arc reactor. *Energy* 34 (2009) 172-177.
- [21] C. Liu, A. Marafee, B. Hill, G. Xu, R. Mallinson, L. Lobban. Oxidative coupling of methane with ac and dc corona discharges. *Industrial & Engineering Chemistry Research* 35 (1996) 3295-3301.
- [22] N. Rueangjitt, W. Jittiang, K. Pornmai, J. Chamnanmanoontham, T. Sreethawong, S. Chavadej. Combined reforming and partial oxidation of CO₂-containing natural gas using an AC multistage gliding arc system: effect of number of plasma reactors. *Plasma Chemistry and Plasma Processing* 29 (2009) 433-453.

- [23] K. Supat, S. Chavadej, L.L. Lobban, R. Mallinson. Combined steam reforming and partial oxidation of methane to synthesis gas under electrical discharge. *Industrial & Engineering Chemistry Research* 42 (2003) 1654-1661
- [24] K. Pornmai, H. Sekiguchi, S. Chavadej. Synthesis gas production from reforming of CO₂-containing natural gas with steam using an AC gliding arc discharge system: effects of steam addition in feed and operational parameters. *Plasma Sources Science and Technology* (In Contribution).
- [25] T. Zielinski, J. Kijenski. Plasma carbon black the new active additive for plastic. *Composites Part A : Applied Science and Manufacturing* 36 (2005) 467-471.
- [26] T. Opalinska, T. Zielinski, K. Schmidt-Szalowski. Carbon black generation in gliding arc discharges. *Polish Journal of Chemistry* 77 (2003) 1357-1361.
- [27] K. Supat, A. Kruapong, S. Chavadej, L.L. Lobban, G.R. Millinson. Synthesis gas production from partial oxidation of methane with air in AC electric gas discharge. *Energy & Fuels* 17 (2003) 471-481.